

# Application of nonlinear models to estimate the gain of one-dimensional free-electron lasers

E. Peter<sup>1,†</sup>, F. B. Rizzato<sup>1,†</sup> and A. Endler<sup>1</sup>

<sup>1</sup>Instituto de Física, Universidade Federal do Rio Grande do Sul, Caixa Postal 15051, 91501-970, Porto Alegre, RS, Brasil

(Received 10 November 2016; revised 23 April 2017; accepted 24 April 2017)

In the present work, we make use of simplified nonlinear models based on the compressibility factor (Peter *et al.*, *Phys. Plasmas*, vol. 20 (12), 2013, 123104) to predict the gain of one-dimensional (1-D) free-electron lasers (FELs), considering space-charge and thermal effects. These models proved to be reasonable to estimate some aspects of 1-D FEL theory, such as the position  $z$  of the onset of mixing, in the case of a initially cold electron beam, and the position  $z$  of the breakdown of the laminar regime, in the case of an initially warm beam (Peter *et al.*, *Phys. Plasmas*, vol. 21 (11), 2014, 113104). The results given by the models are compared to wave-particle simulations showing a reasonable agreement.

**Key words:** plasma applications, plasma devices

---

## 1. Introduction

Free-electron lasers (FELs) have a special place inside the world of coherent electromagnetic waves sources: their tunability is one of their most important theoretical features. These devices are able to generate radiation in a wide range of wavelengths, from microwaves to X-rays. The FEL tunability is possible by adjusting some parameters and initial conditions, such as the electron beam energy, the wiggler wavelength and the wiggler field strength (Bonifacio *et al.* 1990).

In a FEL, a seed of radiation (the laser) co-propagates with a relativistic electron beam accelerated by a particle accelerator. The beam enters a time independent and spatially periodic magnetic field generated by an undulator or a wiggler and the particles interact with the laser and wiggler fields as well as with themselves through space-charge forces. The superposition of the laser and wiggler fields forms the so called ponderomotive potential. This potential confines the electrons. If the resonance condition is satisfied, the electrons lose energy and form micro-bunches separated by a distance  $d = 2\pi/k_p$ , where  $k = 2\pi/\lambda$  and  $k_w = 2\pi/\lambda_w$  are the wavenumber of the laser and the wiggler, respectively and  $k_p = k + k_w$ . The energy lost by the electrons is transferred to the laser (Kroll & McMullin 1978; Sprangle, Tang & Manheimer 1980; Marshall 1985; Murphy, Pellegrini & Bonifacio 1985; Bonifacio *et al.* 1990; Brau 1990; Freund & Antonsen 1996; Seo & Choi 1997). However, experimentally, due to

† Email addresses for correspondence: [peterpeter@uol.com.br](mailto:peterpeter@uol.com.br), [rizzato@if.ufrgs.br](mailto:rizzato@if.ufrgs.br)

the interaction between the particles and the fields, the operability of the machines is limited in terms of the electron beam properties, for example (Allaria *et al.* 2012).

According to the resonance condition, approximately given by  $\gamma_r = \sqrt{\lambda_w(1 + a_w^2)}/2\lambda$ , ( $\gamma_r$  is the resonant Lorentz factor;  $a_w = e\lambda_w B_w/2\pi mc^2$  is the adimensional undulator parameter;  $B_w$  is the magnetic field strength;  $m$  and  $e$  are the electron's rest mass and charge; and  $c$  is the speed of light) if we decrease the value of the laser wavelength, the resonant energy,  $E_r \equiv m\gamma_r c^2$ , increases. The wiggler wavelength corresponds to the spatial periodicity of the magnetic field generated by the wiggler, which in turn is the distance between magnets with the same magnetic orientation.

As the system is conservative, the total energy of the system must be conserved – part of the total energy is the sum of the kinetic energy of each electron of the beam and the another part is the energy associated with the electromagnetic mode. For a FEL, it is desirable to maximize the energy transfer to the laser. As in many amplifiers, the gain is one way to evaluate how good the amplifier is. The gain is defined as the ratio of the final to the initial amplitudes of the laser. It is usually measured in a decibel scale and the typical range of it is approximately tens of dB. The purpose of this work is to use the nonlinear models recently developed (Peter *et al.* 2013; Peter, Endler & Rizzato 2014, 2016) to estimate the theoretical gain of one-dimensional (1-D) FELs in a single pass and time-independent (steady-state regime) configuration, both for Compton and Raman regimes. In the Compton regime, the system dynamics is mainly driven by the ponderomotive potential, while in the Raman regime, the space-charge effects are comparable to the ponderomotive potential. The predicted results are compared to wave–particle simulations.

The paper is organized as follows: in § 2, we present the physical model; in § 3, we show the nonlinear model predictions for an initially cold beam and we make a comparison with the results obtained through wave–particle simulations and the results are compared with those available in literature; in § 4, we compare the results given by the wave–particle simulations and the results given by energies; and in the nonlinear model for an initially water bag distribution for the electrons § 5, we draw our conclusions.

## 2. Physical model

The physical model presented in this work has been developed in a previous paper (Peter *et al.* 2013). Thus, only the final expressions for the equations are shown.

The wiggler ( $A_w$ ) and the laser ( $A$ ) fields are described by their vector potentials fields, respectively

$$\frac{eA_w}{mc^2} = a_w(z) \hat{e} \exp[i(k_w z)] + \text{c.c.}, \quad (2.1)$$

$$\frac{eA}{mc^2} = a(z) \hat{e} \exp[i(kz - \omega t)] + \text{c.c.}, \quad (2.2)$$

$\omega$  is the frequency of the radiation;  $a = a(z)$  is the slowly varying dimensionless amplitude of the laser and  $a_w$  is the dimensionless undulator parameter;  $z$  is the position of the beam; and  $\hat{e}$  is the circular polarization vector.

The 1-D FEL dynamics is well described by particle equations for the energy  $\gamma$  and phase  $\theta$  ( $= [k + k_w]z - \omega t$ ), and the wave equation for the laser amplitude  $a(z)$ . These equations form what is called wave–particle system, composed by  $2N + 2$  equations, where  $N$  is the number of particles (in the present paper we considered 1000 particles

for the cold beam case and 5000 particles for the warm beam case). The equations, shown below, were solved using the LSODE code (Hindmarsh 1980, 1983) and they were normalized in a way that:  $t = \omega t$ ,  $v = v/c$  and  $z = v_p t = k/(k + k_w)t$

$$\frac{d}{dz} \gamma_j = -\frac{a_w}{2\gamma_j} [ae^{i\theta_j} + \text{c.c.}] + \eta^2 v_p v_{z,j} \left\langle -(\theta_k - \theta_j) + \pi \frac{(\theta_k - \theta_j)}{|\theta_k - \theta_j|} \right\rangle, \quad (2.3)$$

$$\frac{d}{dz} \theta_j = \frac{v_{z,j}}{v_p (1 - v)} - 1, \quad (2.4)$$

$$\frac{d}{dz} a = \eta^2 v_p a_w \left\langle \frac{e^{-i\theta}}{2\gamma} \right\rangle - i\eta^2 v_p \left\langle \frac{1}{2\gamma} \right\rangle a. \quad (2.5)$$

In these equations,  $j$  is the index for each particle, while the index  $k$  refers to the other particles; the brackets indicate an average over the particle distribution (thus, there is an equation of energy and an equation of phase for each particle); the quantity  $\eta$  is the space-charge factor arising from the beam charge,  $\eta^2 = \omega_p^2/\omega^2$ , with  $\omega_p = \sqrt{4\pi n_0 e^2/m}$  being the plasma frequency and  $n_0$  is the average density of particles; the velocity of the ponderomotive potential is represented by  $v_p = k/(k_w + k) = k/k_p < 1$ ;  $v$  is the detuning, which is a dimensionless parameter that measures somehow the difference between the ponderomotive potential velocity ( $v_p$ ) and the beam velocity ( $v'_p$ ):  $v = (v'_p - v_p)/v'_p$ ; and the longitudinal particle velocity is given through the relativistic Lorentz factor definition:  $v_{z,j} = [1 - (1 - |a_{tot}|^2)/\gamma_j^2]^{1/2}$ , with  $|a_{tot}|^2 = |a_w(\exp[i(k_w z)] + \text{c.c.}) + (a \exp[i(kz - \omega t)] + \text{c.c.})|^2$ .

The total energy of the system is conserved while the system evolves. Dividing the energy by a volume and using the Poynting vector is possible to find a relation in which the density of energy is conserved ( $n_0 \langle \gamma \rangle mc^2 + |E|^2/4\pi = \epsilon^* = \text{const.}$ , where  $|E|$  is the modulus of the electric field of the laser) (Bonifacio *et al.* 1990). This relation is rewritten in terms of the variables defined in this section as  $\eta^2 \langle \gamma \rangle + |a|^2 = \epsilon$ .

The evolution of the laser amplitude is well described by the models, both for the initially cold and warm beam in the linear regime. Some considerations are made to evaluate the gain (its maximum is measured taking the first peak of the laser amplitude). The gain,  $\Gamma$ , is defined with help of a decibel scale as

$$\Gamma(z) = 10 \log \left( \frac{|a(z)|}{|a(z=0)|} \right). \quad (2.6)$$

The theoretical gain given by wave-particle equations is compared to the models prediction in the next sections.

### 3. Cold beam

The first case analysed in this paper is the initially cold beam case. It implies that at  $z=0$  all of the particles of the beam have the same velocity ( $v'_p$ ) and energy ( $\gamma_r$ ). As shown in a previous work (Peter *et al.* 2013), the onset of mixing takes place in the phase space when the local electron density, at the position of the onset, goes to infinity. Then, the compressibility factor (which is defined as  $C \propto n_0/n$ , where  $n$  is the local density) goes to zero. This occurs because the distribution of the particles becomes a multi-valued function. A very similar model was recently applied to the case of magnetically focused beams as well (Souza *et al.* 2010).

In the model, the complete set of equations, given by equations (2.3)–(2.5), is linearized as in Bonifacio *et al.* (1990). Thus, the linear evolution of the radiation field is obtained through the integration of the following set of equations (where dot indicates time derivation)

$$\dot{X} = i \left[ \frac{a_w}{2v_p^2(1-\nu)\gamma_r^2} \right] \tilde{a} + \left[ \frac{1+a_w^2}{v_p^2(1-\nu)\gamma_r^3} \right] Y, \quad (3.1)$$

$$\dot{\tilde{a}} = - \left[ v_p \frac{a_w \eta^2}{2\gamma_r} \right] \left( iX + \frac{Y}{\gamma_r} \right) - i \left( v_p \frac{\eta^2}{2\gamma_r} - \nu \right) \tilde{a}, \quad (3.2)$$

$$\dot{Y} = - \frac{a_w}{2\gamma_r} \tilde{a} - v_p^2 \eta^2 X + \dot{Y}|_{therm}, \quad (3.3)$$

where the collective complex variable  $X$  represents the fluctuations in the phase ( $X = \langle e^{-i\tilde{\theta}_0} \delta\tilde{\theta} \rangle$ ), while the subscript 0 refers to the initial condition and  $\delta\tilde{\theta} = \tilde{\theta} - \tilde{\theta}_0$ ; the collective complex variable  $Y$  represents the fluctuations in the energy ( $Y = \langle e^{-i\tilde{\theta}_0} \delta\gamma \rangle$ ) and  $\delta\gamma = \gamma - \gamma_0$ ;  $\tilde{a}$  is the transformed complex laser amplitude ( $\tilde{a}e^{i\tilde{\theta}} = ae^{i\theta}$ ); and,  $\tilde{\theta}$  is the transformed phase ( $\theta = \tilde{\theta} - \nu z$ ); the subscript  $r$  refers to the resonance condition; in the case of a cold beam  $\dot{Y}|_{therm} = 0$ : this term will be explained later (this term is added due to thermal effects).

With these coupled equations it is possible to generate a third-order polynomial equation to determine the parameters that lead to the maximum growth rate and the instability limits. The linear set of equations also provides the linear growth of the laser amplitude. In Bonifacio *et al.* (1990), for example, the linear growth rate is analysed including space-charge effects.

But the linear set of equations itself is unable to predict the onset of the phase-space mixing. In the model, the nonlinearities of the space-charge effects are introduced due to a connection between the phase and the energy. By exploring this connection, a second-order ordinary differential equation for the phase, which depends on the initial phase,  $\tilde{\theta}_{0j}$ , is written as

$$\frac{d^2}{dz^2} \tilde{\theta}_j = -\chi_1 (\tilde{a}e^{i\tilde{\theta}_j} + \text{c.c.}) + \chi_2 (\tilde{\theta}_{0j} - \tilde{\theta}_j), \quad (3.4)$$

where  $\chi_1 \equiv a_w(1+a_w^2)/(2v_p^2(1-\nu)\gamma_r^4)$  and  $\chi_2 \equiv \eta^2(1+a_w^2)/((1-\nu)\gamma_r^3)$ .

Deriving (3.4) with respect to  $\tilde{\theta}_0$ , and defining  $\partial\tilde{\theta}_j/\partial\tilde{\theta}_0 \equiv C$  as the compressibility factor, we obtain an evolution equation that indicates the beginning of the phase mixing (it occurs in the model when the first  $\tilde{\theta}_0$  satisfies the condition  $C \rightarrow 0$ ). The equation of the compressibility evolution is given by

$$\frac{d^2}{dz^2} C = -i\chi_1 (\tilde{a}e^{i\tilde{\theta}_j} - \text{c.c.}) + \chi_2 (1 - C). \quad (3.5)$$

The linear equations combined with (3.4) and (3.5) form our simplified model that can estimate the position  $z$  and  $\theta$  of the onset of mixing, the saturated amplitude of the laser and the critical value of  $\nu$  responsible to separate Compton and Raman regimes (Peter *et al.* 2013). These equations are solved also using the LSODE code (Hindmarsh 1980, 1983).

In the model, the position  $z$  of the onset of mixing is obtained when the first  $\tilde{\theta}_0$  satisfies the condition  $C \rightarrow 0$ : this position is called  $z_0$ . This point forward, we freeze

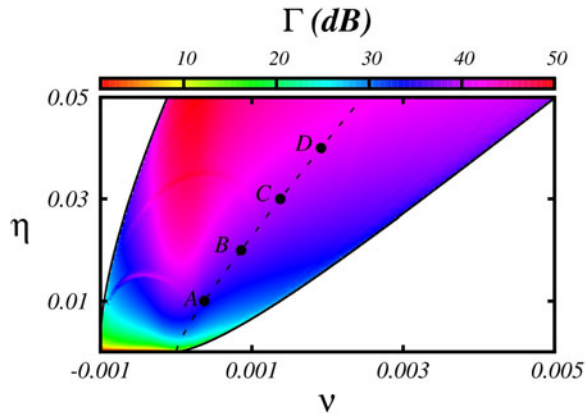


FIGURE 1. Map  $\eta$  versus  $\nu$  of the gain  $\Gamma$ . The colours indicate the gain, in dB. The black solid lines are from the linear analysis and they delimit the instable region. The dashed line is the curve which maximizes the growth rate. Finally, the indexed filled circles are the points used to compare the model and the full simulations results. The commas appear because the gain depends on a combination between the growth rate and the position  $z_0$  of the onset of the mixing.

the collective variables  $X$  and  $Y$ . Thus, the amplitude  $|a|$  oscillates and we take the maximum value of it. This value, obtained through the model, is assumed to estimate the first peak amplitude in the wave–particle simulations.

Figure 1 shows a map of the gain for the model, in terms of  $\nu$  and  $\eta$ . The map was built for  $a_w = 0.5$ ,  $|a(z=0)| = a_w \times 10^{-5}$  and  $v_p = 0.99$  – these values correspond to an initial beam energy of the order of  $\sim 4$  MeV. The black solid lines represent the limits of the instability region, while the dashed line is the maximum growth rate curve obtained from the cubic polynomial of the linear set of equations. The colours indicate the gain and the indexed circles, from A to D, denote the points used to compare the model and the full simulations – and are over the curve of maximum growth rate. The values of the gain vary from 0 to  $\approx 47$  dB and grow by increasing the value of  $\eta$ .

In figure 2, the points from A to D of figure 1 are compared. The horizontal axis represents  $\eta$ , while the vertical axis shows the gain,  $\Gamma$ . The indexed points represent the result from the model, while the solid line is obtained from wave–particle simulations. Until the point A ( $\eta = 0.01$ ) the gain is very sensible to the space-charge effects: the gain is increased by three orders of magnitude (from zero to  $\Gamma = 30$  dB). In this region, the kinetic energy available for the energy conversion increases as  $\eta$  increases. The space-charge effects also increase, but the ponderomotive potential mainly drives the dynamics of the particles. This corresponds to the Compton regime (Peter *et al.* 2013).

After the point A, the gain still grows, but in, according to figure 2, an approximately linear fashion. This occurs because the space-charge effects becomes relevant to the system dynamics. The space-charge effects act against the ponderomotive potential. While the ponderomotive tends to attract the particles (forming micro-bunches), the space charge acts to the contrary. It is typical of Raman or near Raman regimes (Peter *et al.* 2013).

Moreover, the red curve of figure 2 is obtained from a relation described in McNeil & Thompson (2010), Milton *et al.* (2001), Kim (1986) for an initially

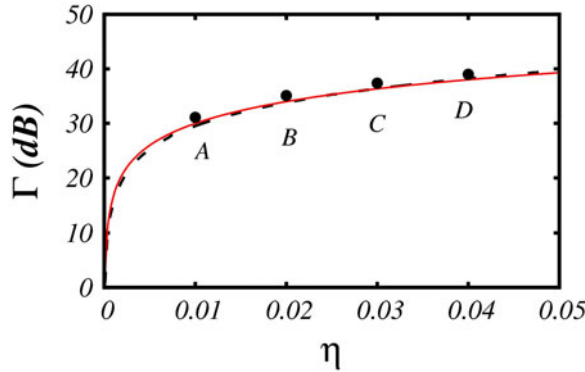


FIGURE 2. The figure depicts the behaviour of  $\Gamma$  versus  $\eta$ . The solid line corresponds to the result from wave–particle simulations, while the filled circles are from the model. The indexed points correspond exactly to the ones of figure 1. The pair  $\eta$  and  $\nu$  is over the maximum growth rate curve. The red curve is the gain considering  $P_{sat} = \rho P_{beam}$ .

cold beam, considering space-charge effects. The relation is given by  $P_{sat} = \rho P_{beam}$ , where  $P_{sat}$  is the saturation power of the laser,  $P_{beam}$  is the beam power and  $\rho$  is the FEL parameter Bonifacio *et al.* (1990), while the gain can be written as  $\Gamma = 10 \log (P_{sat}/P_0)^{1/2}$ , where  $P_0$  is the initial power of the laser. The FEL parameter is written as  $\rho = 1/\gamma_r (a_w \omega_p / 4ck_w)^{2/3}$ . Using the variables transformation proposed in this work, we obtain

$$\Gamma = 10 \log \left[ \frac{\eta^2 \left( \frac{a_w \eta k_w}{4k} \right)^{2/3}}{|a(z=0)|^2} \right]^{1/2}. \tag{3.6}$$

Thus, the red curve agrees very well with the simulations and, consequently, with the simplified model given in this work. The simplified model gave values of the gain higher than the wave–particle simulations of the order of a few per cent. This way, the model agrees well with the wave–particle simulations, proving to be a good tool to estimate the amplification of the laser.

**4. Warm beam**

For a warm beam, at  $z = 0$  we consider that the velocity of the particles is given by a water bag distribution function, where  $\Delta v_0$  is the half-width of the distribution, while the particles distribution in the phase space is spatially homogeneous. The difference, in terms of the wave–particle equations’ integration, consists in a change in the initial conditions of the particles. The evolution of the particles in the phase space occurs in a laminar fashion until nonlinearities begin to dominate the system dynamics. The breakdown of the laminar regime is defined when the lower border of the particle distribution in the phase space becomes a multi-valued function.

Non-relativistic water bag distributions with constant density over the occupied phase space are exactly represented by adiabatic fluid equations (Coffey 1971), while the laminar regime persists. In the model, we consider very small values of velocity

spread – in the hydrodynamical regime, i.e.  $\Delta v_0 < v$ . In this limit, we can use the non-relativistic approximation and the connections between widths in velocity, momentum and energy are approximately linear and their interaction is efficient (Marshall 1985; Brau 1990). This guarantees that if the density is constant in one phase-space representation, then the density is constant in another.

By exploring the connection between (2.3) and (2.4), identifying a pressure term and the thermal effects over the system through the Vlasov equation and its moments (exactly as in Peter *et al.* 2014) and using a relation between the pressure and the initial velocity spread for a non-relativistic water bag distribution given in Coffey (1971) (the relation, although for non-relativistic water bag distribution, is valid for very narrow initial distributions), a linear term that represents the thermal effect in the system is written as

$$\dot{Y}|_{therm} = -\frac{\Delta v_0^2}{2D_{\gamma^2}\gamma_r}X, \tag{4.1}$$

where  $D_{\gamma^2} = \partial^2 v / \partial \gamma^2$ .

In the presence of an initial spread, a pressure term  $\neq 0$  is added to the linear equations. Precisely, (4.1) is replaced in (3.3). The thermal effect acts like the space-charge effect, reducing the linear growth rate. The linear growth rate obtained from this linear set of equations is close to the wave–particle simulations’ growth rate and it is within a range of 6% from calculations in the literature (Chakhmachi & Maraghechi 2009).

The thermal effect must be included in the evolution of the beam element  $\tilde{\theta}_j$ . We do this by preserving the nonlinearities neglected to generate (4.1). This way, (3.4) is changed, giving place to

$$\frac{d^2}{dz^2}\tilde{\theta}_j = -\chi_1(\tilde{a}e^{i\tilde{\theta}_j} + \text{c.c.}) + \chi_2(\tilde{\theta}_{oj} - \tilde{\theta}_j) - \Delta v_0^2 \left[ \frac{\partial \delta \tilde{\theta}_j}{\partial \tilde{\theta}_{oj}} + 1 \right]^{-4} \frac{\partial^2 \delta \tilde{\theta}_j}{\partial \tilde{\theta}_{oj}^2}, \tag{4.2}$$

where  $\delta \tilde{\theta}_j = \tilde{\theta}_j - \tilde{\theta}_0$ .

Differently to (3.4), which is an ordinary differential equation, equation (4.2) is a partial differential equation, which is solved numerically through the finite differences method. The laser amplitude in this equation is given by the integration of the linear system, (3.1)–(3.3) and (4.1), and the equation is solved through the partition of the beam into a large number of discrete elements. Differently to the cold case, in the case of a warm beam, the compressibility factor never goes to zero due the presence of the thermal effects (a similar analysis was made by the group for warm magnetically focused beams (Souza *et al.* 2012)). Then, the breakdown of the laminar regime is reached when density discontinuities are established.

The nonlinear model estimates quite well the peak amplitude of the radiation (Peter *et al.* 2014). If we consider that the breakdown of the laminar regime is located at  $z_b$ , from this point forward, the collective variables  $X$  and  $Y$  are frozen. As in the cold case, the laser dynamics, then, becomes oscillatory. The maximum value of these oscillations correspond to the estimated peak of the radiation field.

Figure 3 shows the gain,  $\Gamma$  against  $\eta$  for  $v_p = 0.99$ ,  $a_w = 0.5$  and  $|a(z=0)| = a_w \times 10^{-5}$  and different values of  $\Delta v_0$ , always over the curve that maximizes the growth rate. The filled circles are from the model, while the lines are from wave–particle simulations. Each colour corresponds to a different value of  $\Delta v_0$ : black is for  $\Delta v_0 = 0.0002$  and red is for  $\Delta v_0 = 0.0008$ .

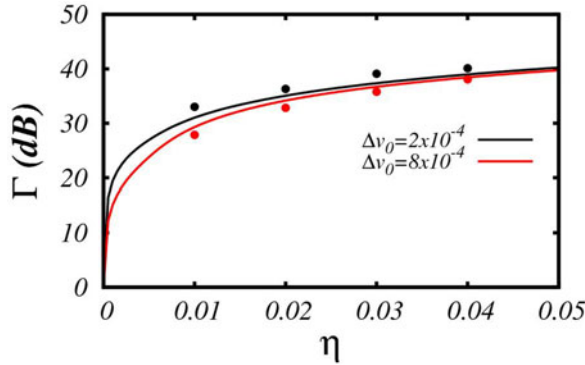


FIGURE 3. In this figure is plotted  $\Gamma$  versus  $\eta$ . The solid line corresponds to the result from the wave–particle simulations, while the filled circles are from the theoretical model. The red (black) ones correspond to  $\Delta v_0 = 0.0008$  ( $\Delta v_0 = 0.0002$ ). The pair  $\eta$  and  $\nu$  is over the maximum growth rate curve.

It is possible to see that the gain is diminished as the initial velocity spread increases. The thermal effect act like the space charge, in opposition to the ponderomotive potential. With the increase of the charge in the system, the thermal effects become less important in the dynamics. Thus, the curves tend to bring together as we increase  $\eta$ . These results agree with what was shown in the previous work (Peter *et al.* 2014).

In figure 4, we plot the gain against the initial velocity spread for a fixed, and small,  $\eta$  ( $\eta = 0.01$ ,  $a_w = 0.5$  and  $|a(z=0)| = a_w \times 10^{-5}$ ). The solid black line was obtained from wave–particle simulations, while the filled circles are from the model. The dashed line is a fit curve of the filled circles.

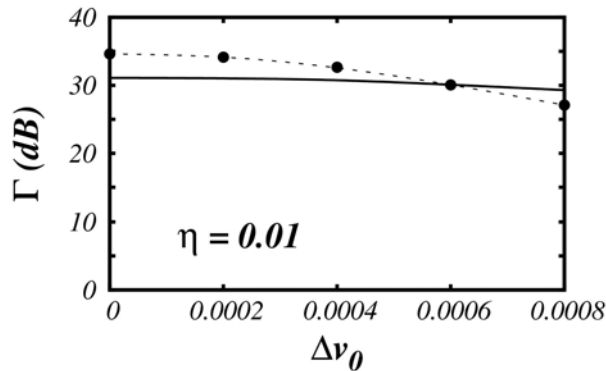


FIGURE 4.  $\Gamma$  is plotted against  $\Delta v_0$  for  $v_p = 0.99$ ,  $\eta = 0.01$ ,  $a_w = 0.5$  and  $|a(z=0)| = a_w \times 10^{-5}$ . The solid line corresponds to the result from the wave–particle simulations, while the filled circles are from the theoretical models. The dashed line is a fit curve for the filled circles. The pair  $\eta$  and  $\nu$  is over the maximum growth rate curve.

As can be seen in figure 4, the model is more sensitive in relation to  $\Delta v_0$  than the wave–particle system. For small values of  $\Delta v_0$ , the oscillations of the laser field in the model are greater than the wave–particle simulations. Thus the model tends



to overestimate the gain in that region. While for values of  $\Delta v_0$  near the limit of the hydrodynamical regime, the model tends to underestimate the gain. This is the effect of the temperature over the model when we freeze the collective variables. The oscillations of the laser field become smaller as we increase  $\Delta v_0$ .

Although the difference is of the order of 15% for the gain for very small  $\Delta v_0$ , the model proved to estimate in a reasonable way the gain obtained from wave-particle simulations and the decreasing tendency of the gain by increasing  $\Delta v_0$ .

## 5. Conclusions

In previous works (Peter *et al.* 2013, 2014), nonlinear models based on the compressibility factor were developed and proven to describe reasonably the dynamics of the FEL, especially the evolution of the laser field in the linear regime. The models were used to determine the parameters to maximize the growth rate of the radiation field and to estimate a number of quantities at the moment of the onset of mixing. In the present work, we applied nonlinear models in order to estimate the gain of the laser field for 1-D FELs in the case of a cold and a warm electron beam. In the cold beam case, a linear set of equations was obtained through the introduction of the collective complex variables  $X$  and  $Y$  and the linearization of the wave-particle equations. The linearized equations emulate the evolution of the laser field in the linear regime. The nonlinear effects, such as the space charge, were introduced by exploring a connection between the phase and the energy of the particles. It allowed us to obtain a second-order ordinary differential equations for the compressibility factor (which is the inverse of the longitudinal density). The zeroes of the compressibility factor indicate the onset the mixing. This point forward, the collective variables are frozen and we take the maximum value of the oscillatory dynamics of the laser field to estimate the gain in the model. We run the simulations for  $a_w = 0.5$  and different values of  $\eta$ , over the curve of maximum growth rate. As shown in the present work, the results of the simplified model agrees well with the wave-particle simulations and with previous works which gave estimations for the gain for an initially cold beam.

Analogously, for the warm beam case, we ran simulations for  $a_w = 0.5$  and different values of  $\eta$  and  $\Delta v_0$ , also over the curve of maximum growth rate. We considered only the hydrodynamical regime (Davidson & Qin 2001) for the nonlinear model. In this regime, a non-relativistic water bag distribution with constant density over the phase space is exactly represented by the adiabatic fluid equations, as long as the laminar regime persists. Then, the electron beam is treated as a fluid. Moreover, the smallness of the initial spread, a typical situation for FELs (Chakhmachi & Maraghechi 2009), allows us to change the phase-space representation. In the nonlinear model for the warm beam case, the laser field is emulated by the linear set of equations (but in this case, a pressure term is added in the equations for the fluctuations of the energy of the particles,  $\dot{Y}|_{therm}$ ). In order to estimate the gain, we let the system evolve and, when discontinuities appear in the density plot (the compressibility factor never goes to zero due to the pressure of the fluid), we freeze the collective and complex variables  $X$  and  $Y$ . Thus, the laser amplitude oscillates and we take the peak value. The results are satisfactory. We have shown that if we increase the thermal effects, i.e. if we increase  $\Delta v_0$ , the gain is reduced gradually and if we increase  $\eta$ , then the role of the pressure term becomes less important. It occurs because the space-charge effect becomes more expressive than the effect of the initial distribution. We emphasize that our simplified model is an alternative way to estimate the gain in FELs, especially in the case of an initially warm beam.

The nonlinear models suggest a way to estimate more features of the FEL, such as the density of particles in the position of the breakdown of the laminar flow and the fraction of particles actively participating in the FEL interaction process. Other initial distributions can be described by a sum of water bag distributions in the hydrodynamical regime. These topics are of relevance in the study of the FEL theory and they shall be developed in future works.

### Acknowledgements

This work was supported by CNPq and FAPERGS, Brazil, and by the Air Force Office of Scientific Research (AFOSR), USA, under the grant FA9550-12-1-0438. The authors wish to thank useful discussions with R. Pakter, S. Marini and A. Serbeto.

### REFERENCES

- ALLARIA, E., BATTISTONI, A., BENCIVENGA, F., BORGHES, R., CALLEGARI, C., CAPOTONDI, F., CASTRONOVO, D., CINQUEGRANA, P., COCCO, D., CORENO, M. *et al.* 2012 Tunability experiments at the fermi@elettra free-electron laser. *New J. Phys.* **14**, 113009.
- BONIFACIO, R., CASAGRANDE, F., CERCHONI, G., DE SALVO SOUZA, L., PIERINI, P. & PIOVELLA, N. 1990 Physics of the high-gain fel and superradiance. *Riv. del Nuovo Cimento* **13** (9), 1–69.
- BRAU, C. 1990 *Free-Electron Lasers*. Academic.
- CHAKHMACHI, A. & MARAGHECHI, B. 2009 Stability properties of free-electron laser in Raman regime with thermal electron beam. *Phys. Plasmas* **16** (4), 043110.
- COFFEY, T. P. 1971 Breaking of large amplitude plasma oscillations. *Phys. Fluids* **14** (7), 1402–1406.
- DAVIDSON, R. C. & QIN, H. 2001 *Physics of Intense Charged Particle Beams in High Energy Accelerators*. World Scientific.
- FREUND, H. P. & ANTONSEN, T. M. 1996 *Principles of Free-Electron Lasers*. Chapman and Hall.
- HINDMARSH, A. C. 1980 Lsode and lsodi, two new initial value ordinary differential equation solver. *ACM SIGNUM Newsletter* **15** (4), 10–11.
- HINDMARSH, A. C. 1983 ODEPACK, A systematized collection of ODE solvers. In *Scientific Computing* (ed. R. S. Stepleman *et al.*), IMACS Transactions on Scientific Computation, vol. 1, pp. 55–64. North Holland Publishing Co.
- KIM, K.-J. 1986 Three-dimensional analysis of coherent amplification and self-amplified spontaneous emission in free-electron lasers. *Phys. Rev. Lett.* **57**, 1871–1874.
- KROLL, N. M. & MCMULLIN, W. A. 1978 Stimulated emission from relativistic electrons passing through a spatially periodic transverse magnetic field. *Phys. Rev. A* **17** (7), 300–308.
- MARSHALL, T. C. 1985 *Free-Electron Lasers*. Macmillan Publishing Company.
- MCNEIL, B. W. J. & THOMPSON, N. R. 2010 X-ray free-electron lasers. *Nature Photonics* **4**, 814–821.
- MILTON, S. V., GLUSKIN, E., ARNOLD, N. D., BENSON, C., BERG, W., BIEDRON, S. G., BORLAND, M., CHAE, Y.-C., DEJUS, R. J., DEN HARTOG, P. K. *et al.* 2001 Exponential gain and saturation of a self-amplified spontaneous emission free-electron laser. *Science* **292** (5524), 2037–2041.
- MURPHY, J. B., PELLEGRINI, C. & BONIFACIO, R. 1985 Collective instability of a free electron laser including space charge and harmonics. *Opt. Commun.* **53** (3), 197–202.
- PETER, E., ENDLER, A. & RIZZATO, F. B. 2014 Nonlinear model for thermal effects in free-electron lasers. *Phys. Plasmas* **21** (11), 113104.
- PETER, E., ENDLER, A. & RIZZATO, F. B. 2016 Growth rate for free-electron lasers through a warm beam layered model. *J. Plasma Phys.* **82**, 905820307.
- PETER, E., ENDLER, A., RIZZATO, F. B. & SERBETO, A. 2013 Mixing and space-charge effects in free-electron lasers. *Phys. Plasmas* **20** (12), 123104.
- SEO, Y. & CHOI, E. H. 1997 A submillimeter Raman free-electron laser in a dense plasma background. *IEEE Trans. Plasma Sci.* **25** (2), 360–363.

- SOUZA, E. G., ENDLER, A., PAKTER, R., RIZZATO, F. B. & NUNES, R. P. 2010 The controlling role of envelope mismatches in intense inhomogeneous charged beams. *Appl. Phys. Lett.* **96**, 141503.
- SOUZA, E. G., ENDLER, A., RIZZATO, F. B. & PAKTER, R. 2012 Adiabatic-nonadiabatic transition in warm long-range interacting systems: the transport of intense inhomogeneous beams. *Phys. Rev. Lett.* **109**, 075003.
- SPRANGLE, P., TANG, C.-M. & MANHEIMER, W. M. 1980 Nonlinear theory of free-electron lasers and efficiency enhancement. *Phys. Rev. A* **21**, 302–318.